Optical and Magnetic Properties of PbTe(Ni)

N. Romčević[a,*], J. Trajić[a], M. Romčević[a], D. Stojanović[a], T.A. Kuznetsova[b],

D.R. Khokhlov[b] W. Dobrowolski[c], R. Rudolf[d,e], and I. Anžel[d]

[a]Institute of Physics, Pregrevica 118, 11080 Belgrade, Serbia

[b]Moscow State University, 119899 Moscow, Russia

[c]Institute of Physics, Polish Academy of Sciences, al. Lotników 32/46, 02-668 Warszawa, Poland

[d]Faculty of Mechanical Engineering, University of Maribor, Smetanova 17, 2000 Maribor, Slovenia

[e]Zlatarna Celje d.d., Kersnikova 19, 3000 Celje, Slovenia

Far-infrared and magnetic properties of Ni doped PbTe ($Z_{Ni} = 1 \times 10^{19}$ at./cm^3) single crystal are investigated in a broad range of temperature and magnetic fields. Far-infrared reflection spectra were analyzed using a fitting procedure based on the modified plasmon–two phonon interaction model. Together with the strong plasmon–two longitudinal optical phonon coupling we obtained a local mode of Ni at about 180 cm^{-1}. This mode intensity depends on temperature. Magnetic measurements shows that PbTe alloys doped with Ni reveals weak ferromagnetic interaction between magnetic ions.

PACS numbers: 63.20.−e, 63.20.Kr, 78.30.−j

1. Introduction

The doping of $A^{IV}B^{VI}$ semiconductor compounds with transition metal impurities has significant scientific and practical interest due to the new materials preparing possibilities. Lead telluride (PbTe) belongs to the $A^{IV}B^{VI}$ IR-sensitive narrow-gap semiconductors group, which acquire new properties in the consequence of doping [1, 2]. Transition metals behave either as donors (Cr, Co, Ni) [3] or neutrals (Mn) [4]. For example, when PbTe is doped with chromium, free carrier concentration n increases to 1.3×10^{19} cm^{-3} and remains unchanged with further increase in the Cr concentration, up to the chromium solubility limit. In the case of most IV–VI diluted magnetic semiconductors (DMS) deviation from stoichiometry (metal vacancies) results in the carrier density sufficiently high to produce strong ferromagnetic interactions between the localized spins. The carrier concentration can be controlled in a wide range by thermal annealing or doping.

In this paper we present far-infrared and magnetic measurements of Ni doped PbTe single crystal sample.

2. Sample and experiment

Single crystal of PbTe(Ni) was grown by the Bridgman method. The impurity concentration in the starting mixture was 3.3×10^{20} at./cm^3. The Ni concentration in the crystal used here was 1×10^{19} at./cm^3, de-

termined by chemical analysis [5]. The structural characteristics were obtained by the X-ray diffraction powder technique. The unit cell was calculated by the least squares methods. All the registered reflections corresponded to PbTe crystals and gave the parameter of the cubic unit cell of $a = 0.6455(3)$ nm, which are in good agreement with values cited in literature [6]. The dislocation density were $(5–7) \times 10^{-4}$ cm^{-2}, registered by selective etching [7]. The Hall effect and conductivity measurements showed that the crystal exhibit n-type conductivity with room-temperature electron concentration of 6×10^{16} cm^{-3}. The far-infrared measurements were carried out with a BOMEM DA-8 FIR spectrometer. A deuterated triglycine sulfate (DTGS) pyroelectric detector was used to cover the wave number range from 40 to 500 cm^{-1}. The magnetic measurements were performed using Lake Shore 7229 AC susceptometer/DC magnetometer.

3. Results and discussion

The far-infrared reflection spectra of the Ni-doped PbTe single crystal sample are shown in Fig. 1a. The experimental data are represented by circles. In the observed sample a concentration of free carriers is high, plasma minimum occurs on higher wave numbers and the phonon structure is screened. In principle, the spectra might be interpreted with the help of a frequency dependent dielectric function with not less than three classical oscillators corresponding to the transversal optical (TO) modes superimposed by the Drude part taking into account the free-carrier contribution. In this way the fit
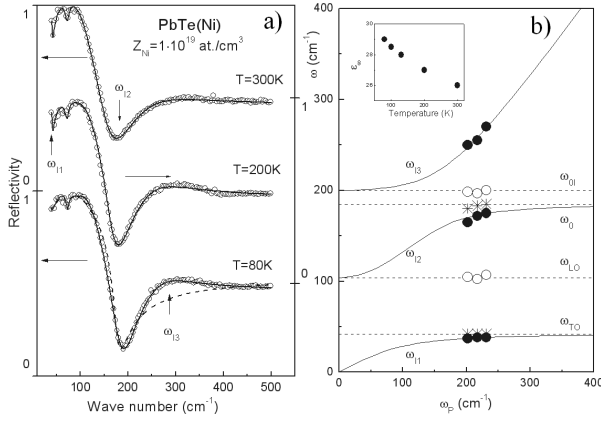
---
* corresponding author; e-mail: romcevi@phy.bg.ac.yu

Fig. 1. (a) Far-infrared reflection spectra of PbTe(Ni) single crystal. Experimental spectra are presented by circles. The solid lines are calculated spectra obtained by a fitting procedure based on the model given by Eq. (1). (b) The eigenfrequencies of the plasmon–two LO phonon modes: the solid and dashed lines are calculated spectra obtained by appliance of model given by Eq. (4) for $n = 2$, and $n = 1$, respectively; • — eigenfrequency spectra ω_{lj} obtained by Eq. (1); ○ — calculated values for ω_{LO} and ω_{0l} (Eq. (3)) and * — experimentally determined values for ω_{TO} and ω_0. Inset: high frequency dielectric constant (ε_∞) vs. temperature.

immediately yielded the TO mode frequencies. Longitudinal optical (LO) modes are determined by the maximum of the dielectric loss function.

In our case the pure LO modes of the lattice are strongly influenced by the plasmon mode (ω_P) of the free carrier. As a result, a combined plasmon–LO phonon mode should be observed [8]. Therefore, the determination of LO mode is connected with the elimination of free carrier influence. Impurity local modes (ω_0) have the same behavior. Considering this fact, we have decided that in analysis of experimental results in Fig. 1a we will use a dielectric function that takes into account the existence of plasmon–two LO phonon interaction [9]. The lines in Fig. 1a were obtained using a dielectric function

$$\varepsilon(\omega) = \varepsilon_\infty \frac{\prod_{j=1}^{n+1}\left(\omega^2 + i\gamma_{lj}\omega - \omega_{lj}^2\right)}{\omega\left(\omega + i\gamma_P\right)\prod_{i=1}^{n}\left(\omega^2 + i\gamma_{ti}\omega - \omega_{ti}^2\right)}$$
$$\times \prod_{k=1}^{s} \frac{\omega^2 + i\gamma_{kLO} - \omega_{kLO}^2}{\omega^2 + i\gamma_{kTO} - \omega_{kTO}^2}. \tag{1}$$

The first term in Eq. (1) represents coupling of plasmon and n phonons, and the second term represents uncoupled modes of the crystal (s). In our case $n + s = 3$. The ω_{lj} and γ_{lj} parameters of the first numerator are eigenfrequencies and damping coefficients of the longitudinal plasmon–n phonon waves. The parameters of the first denominator correspond to the similar characteristics of the transverse (TO) vibrations, where ω_{t1} corresponds to TO mode frequency of PbTe, and ω_{t2} corresponds to ω_0 vibrations of local phonons. In the second term ω_{LO} and ω_{TO} are the longitudinal and transverse frequencies, while γ_{LO} and γ_{TO} are damping. Therefore, the determination of LO-mode and plasma frequency is connected with the decoupled procedure. If the dielectric function defined by Eq. (1) were used, the values of initial ω_{LO}, ω_{0l} and ω_P modes can be determined by (points in Fig. 1b):

$$\omega_P = \frac{\omega_{l1}\omega_{l2}\omega_{l3}}{\omega_{t1}\omega_{t2}}, \tag{2}$$

$$\omega_{LO,0l}^2 = \tfrac{1}{2}\left(\omega_{l1}^2 + \omega_{l2}^2 + \omega_{l3}^2 - \omega_P^2\right) \pm \sqrt{\left(\tfrac{1}{4}\left(\omega_{l1}^2 + \omega_{l2}^2 + \omega_{l3}^2 - \omega_P^2\right)^2 - \omega_{l1}^2\omega_{l2}^2 - \omega_{l1}^2\omega_{l3}^2 - \omega_{l2}^2\omega_{l3}^2 + \omega_P^2\left(\omega_{t1}^2 + \omega_{t2}^2\right)\right)}. \tag{3}$$

In the case of plasmon–two LO phonon coupling, there are three coupled modes (ω_{lj}), which can be calculated by solving the equations (solid lines in Fig. 2):

$$\omega^6 - A\omega^4 - B\omega^2 - C = 0, \tag{4}$$

where:

$$A = \omega_{LO}^2 + \omega_{0l}^2 + \omega_P^2,$$

$$B = \omega_{LO}^2 \times \omega_{0l}^2 + \omega_P^2\left(\omega_{TO}^2 + \omega_0^2\right),$$

$$C = \omega_{TO}^2\omega_0^2\omega_P^2. \tag{5}$$

The agreement of the plasmon-LO phonon mode frequencies calculated on the basis of Eq. (4) with the experimentally ones is very good. Oscillator of a weak intensity, at about 70 cm^{-1} (the second term in Eq. (1)), is a mode from the edge of the Brillouin zone, because the phonon density of PbTe [4] has a maximum at these frequencies. As a result of the best fit we obtained TO frequency (ω_t)

and the frequencies of the coupled modes and then calculated values for ω_{LO}, ω_{0l} and ω_P using Eqs. (2), (3). We determined $\omega_t = 32$ cm^{-1}, $\omega_{LO} = 104$ cm^{-1} and $\omega_0 = 180$ cm^{-1} which is in good agreement with the literature [2, 3]. The oscillators denoted by $j = 1, 2, 3$ in Eq. (1) are the dominant structures in the position of the coupled plasmon–two LO phonon modes. The frequencies of these modes (ω_{lj}, $j = 1, 2, 3$) [9] are marked by arrows (Fig. 1a).

The temperature change of ε_∞ is shown in the inset of Fig. 1b. Decreasing the temperature increases ε_∞. This is in agreement with the theoretical predictions given in Ref. [10] for a cubic crystal without phase transition. Also, the relatively high values of ε_∞ are typical of this kind of materials [11].

Local phonon mode position is estimated in the way we described in Refs. [8, 11]. As the result of the best agreement between experimental and theoretical spectra
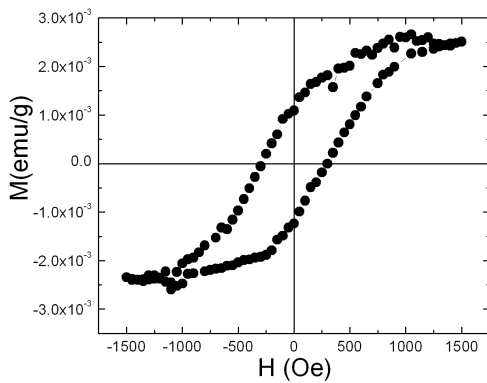
Fig. 2. Magnetization hysteresis loop for PbTe(Ni) at 25 K.

we determined this mode position at 180 cm^{-1}. In order to demonstrate the existence of an additional mode at about 180 cm^{-1}, the calculated spectra with (solid line) and without (dashed) this oscillator are shown in Fig. 1a, for temperature of 80 K. In our opinion, the additional oscillator is related to excitations of local phonon mode in the vicinity of an impurity atom. This conclusion is based on the fact that the additional oscillators have frequencies above the upper end optical range of PbTe $\omega_{LO} = 104$ cm^{-1}. It is known [3, 4] that transition element (Cr, Ni, Co) with small concentration, enters in PbTe lattice as a donor impurity in 3+ state (in our case Ni^{3+}).

Lead telluride grows with rather a high concentration of native defects (vacancies, etc). Ni in PbTe substitutes for Pb. Ni is a substitution impurity ion, so every ion in PbTe is no longer at the center of inversion symmetry and PbTe vibration modes could be both Raman and far-infrared active. The impurity mode can arise simply due to the difference between masses and force constants of the impurity ion and the ion of the host material [12], or their appearance can be caused by more complex mechanism of electron–phonon interaction [11]. In our case, taking into account the change of mass and force constants between an impurity and its surrounding, we have demonstrated that this is the case of the Ni impurity local modes. That is, if the semiconductor is doped with a substitution impurity [12] (in this case Ni), when substitution of the heavier mass (Pb) is made by a lighter impurity, one gets two modes: a local mode situated above the optical band and a gap mode situated above the acoustic band but below the optical band of the host lattice.

In the range of high temperatures the sample is the Curie–Weiss paramagnet with temperature dependence of the magnetic susceptibility described by the Curie–Weiss law. At low temperatures, the transition to ferromagnetic phase takes place and the magnetic hysteresis loop was clearly observed (Figure 2). The remnant polarization was 1.1×10^{-3} emu/g, and coercive field was 295 Oe. This type of materials growing with high deviation from stoichiometry produced rather high concentration of native defect (vacancies, etc.). Since Ni is ferromagnetic, even a small admixture of Ni in PbTe leads to ferromagnetic behavior. The source of ferromagnetism is the Ruderman–Kittel–Kasuya–Yoshida (RKKY) interaction between mobile holes and localized magnetic moments.

4. Conclusion

In this paper, we have shown the far-infrared reflection spectra of Ni doped PbTe ($Z_{Ni} = 1 \times 10^{19}$ at./cm^3) single crystal sample. Together with the strong plasmon–two LO phonon coupling we obtained local mode of Ni at about 180 cm^{-1}. The local phonon mode and plasma frequencies temperature dependences are estimated from the plasmon–phonon interaction, applying represented model (decoupling procedure). Magnetic measurement showed that this system has low-temperature ferromagnetic phase which is mediated by interaction between mobile holes and localized magnetic moments.

References

[1] B.A. Volkov, O.M. Ruchaiskii, *Pis'ma Zh. Eksp. Teor. Fiz.* **62**, 205 (1995) [*JETP Lett.* **62**, 217 (1995)].

[2] D.R. Khokhlov, B.A. Volkov, in: *Proc. 23rd Int. Conf. on the Phys. of Semiconductors, Berlin 1996*, Ed. M. Schefler, Vol. 4, World Sci., Singapore 1996, p. 2941.

[3] B.A. Volkov, D.R. Khoklov, *Physics-Uspekhi* **45**, 819 (2002).

[4] J. Trajić, M. Romčević, N. Romčević, A. Golubović, S. Durić, V.N. Nikiforov, *J. Alloys Comp.* **365**, 89 (2004).

[5] V.P. Zlomanov, T.A. Kuznetsova, S.G. Dorofeev, V.D. Volodin, O.I. Tananaeva, *Crystallogr. Rep.* **47**, (Suppl. 1), 128 (2002).

[6] JCPDS card number 38-1435.

[7] O.N. Krylyuk, A.M. Gas'kov, V.P. Zlomanov, *Vestn. Mosk. Univ., Ser. 2: Khim.* **6**, 571 (1986).

[8] J. Trajić, N. Romčević, M. Romčević, V.N. Nikiforov, *Mater. Res. Bull.* **42**, 2192 (2007).

[9] J. Trajić, N. Romčević, M. Romčević, V.N. Nikiforov, *J. Serb. Chem. Soc.* **73**, 369 (2008).

[10] B.A. Volkov, O.A. Pankratov, *Fiz. Tverd. Tela* **24**, 415 (1982).

[11] N. Romčević, J. Trajić, A.T. Kuznetsova, M. Romčević, B. Hadžić, D.R. Khokhlov, *J. Alloys Comp.* **442**, 324 (2007).

[12] A.A. Maradudin, in: *Solid State Physics*, Eds. F. Seitz, D. Turnbull, Vol. **19**, Academic, New York 1966.